Solubility of Sphene in Siliceous Melts

D. Flanagan[1], J. C. Ayers[1], C. F. Miller[1], E. B. Watson[2], F.J. Ryerson[3]

1) Vanderbilt University, Department of Earth and Environmental Sciences
2) Rensselaer Polytechnic Institute
3) Lawrence Livermore National Laboratory

The importance of sphene

- Sphene records magma evolution through compositional zoning and inclusions.
- The Zr-in-sphene **thermobarometer** provides estimates of magmatic temperature and/or pressure.
- Sphene can be used as a **geochronometer** due to relatively high U concentrations and U/Pb ratios.
- Sphene crystallization dramatically affects melt composition, especially for REE

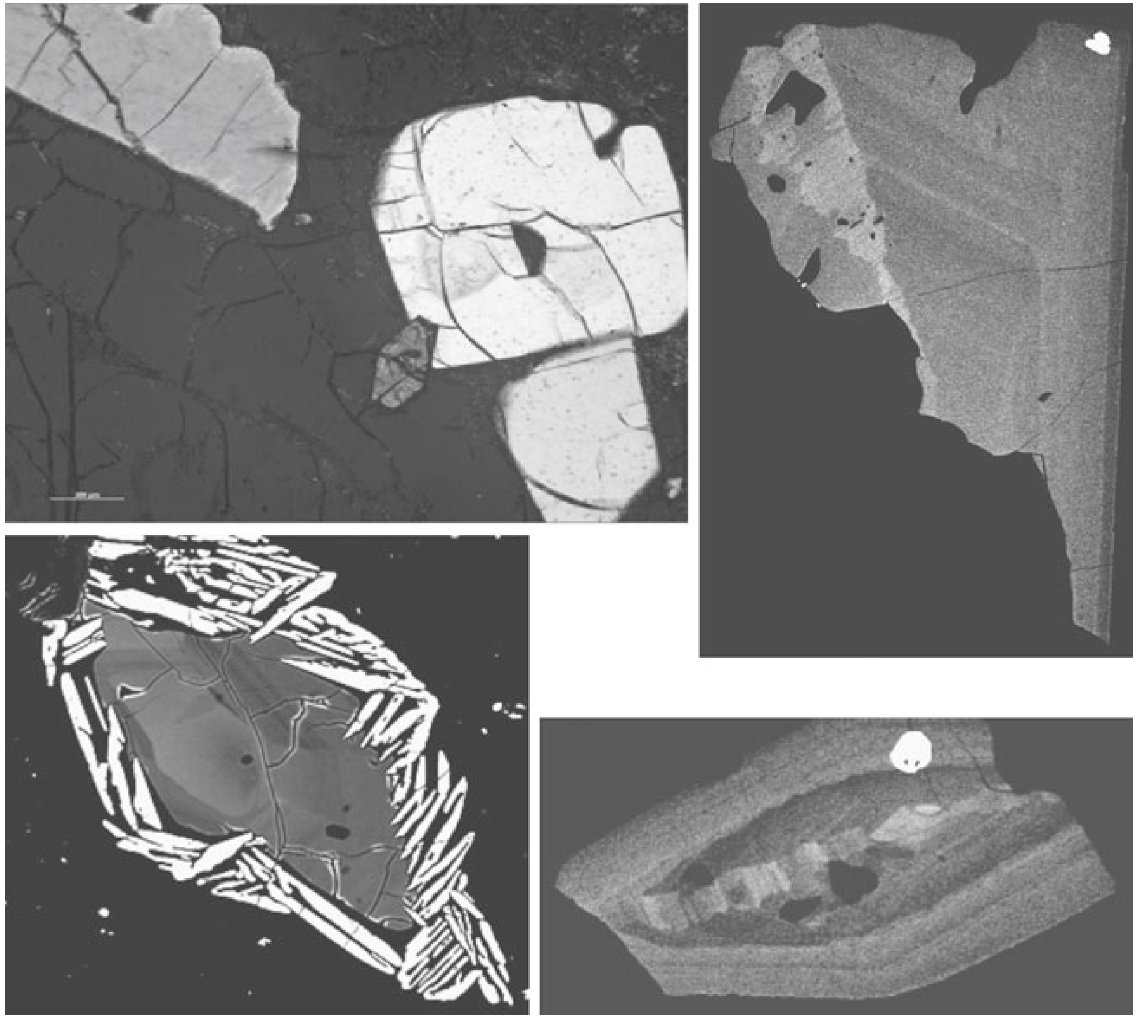

Sphene in Highland Range rhyolites, Colombini et al. (2011)

Sphene influence on melt composition

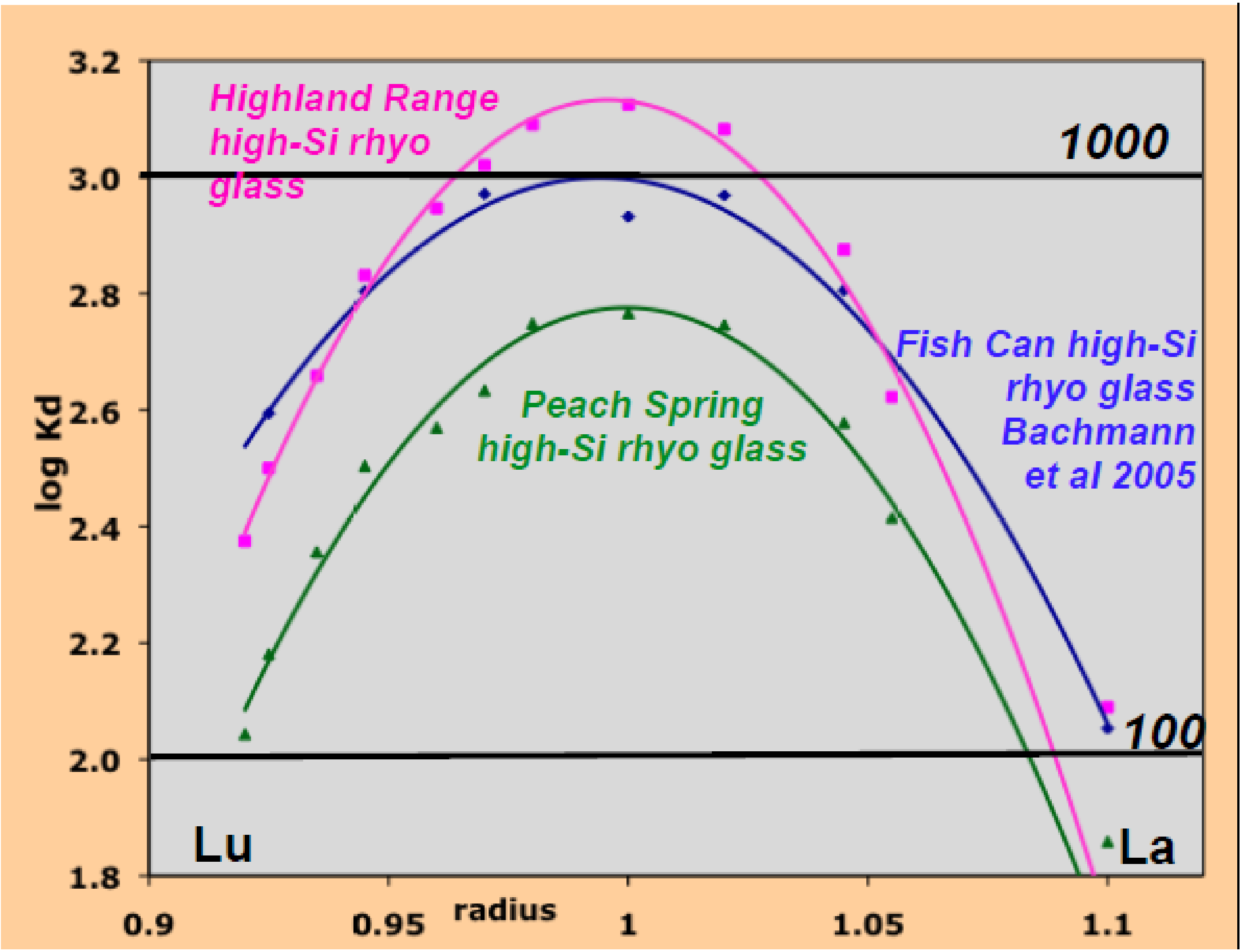

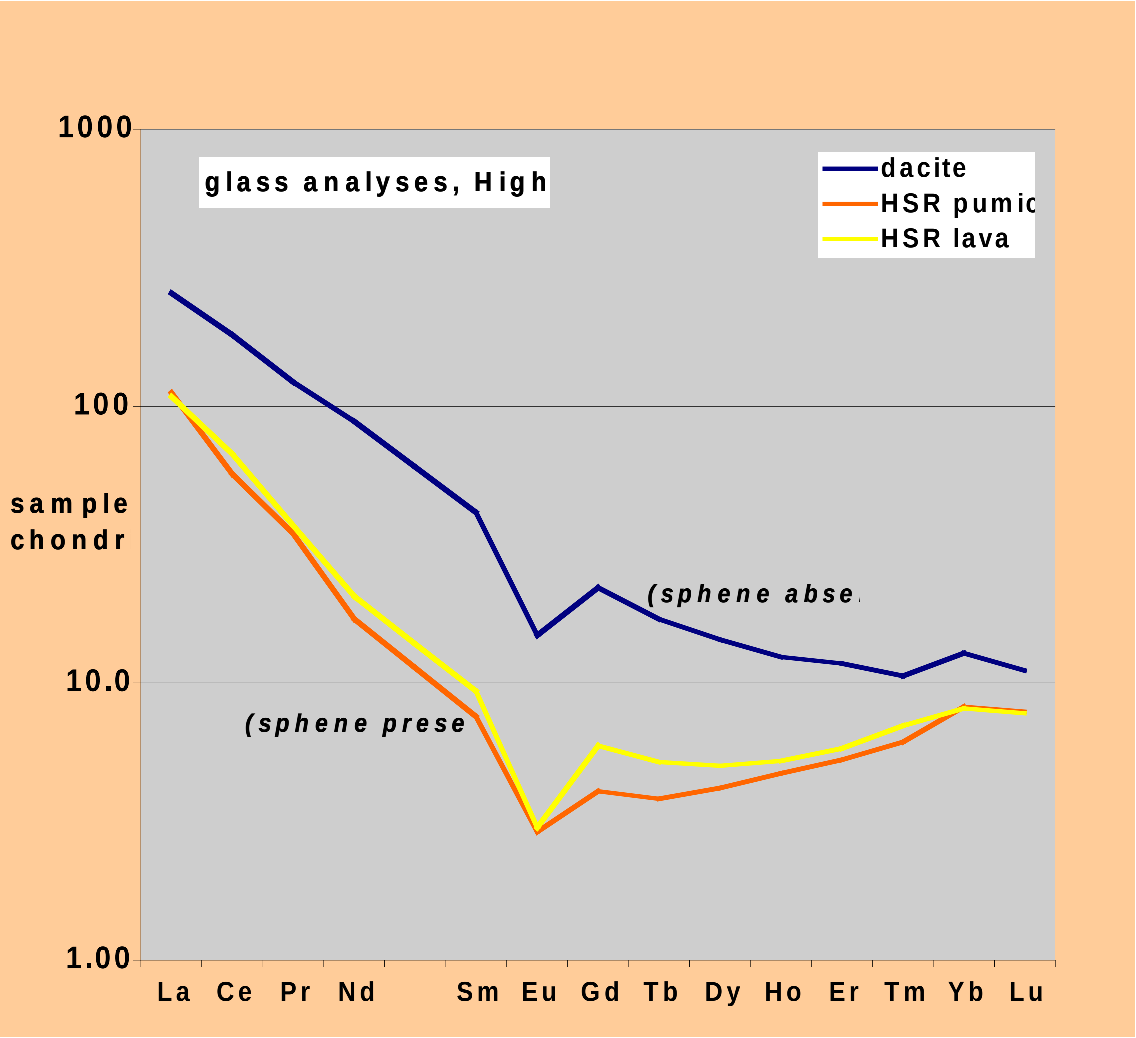

Sphene stability and occurrence

- Sphene most commonly occurs as an accessory mineral in metaluminous, high fO_2, low temperature, high silica igneous rocks.
- Supported by typically low (~710 to 780 ^oC) sphene crystallization temperatures calculated from the Zr-in-sphene thermobarometer (Hayden et al., 2008) and by the restriction of whole-rock middle REE depletion patterns to highly evolved rhyolites and aplites.
- Peraluminous granitoids rarely contain sphene because high Al stabilizes plagioclase, and crystallization of plagioclase removes Ca, suppressing sphene crystallization.

Sphene Solubility

- We lack sufficient data on sphene solubility in siliceous melts to accurately predict when sphene will crystallize in a magmatic system.
- A sphene solubility equation would be useful for:
  - constraining the temperatures of melts
  - determining whether sphene saturation in magmatic source regions is likely
  - determining when sphene can crystallize and begin to exert an influence on melt chemistry.
- We performed sphene growth and dissolution experiments to characterize the dependence of sphene solubility on pressure, temperature, and melt composition.

Anhydrous compositions of starting materials for growth experiments

	PST	PST + GSP	GSP(1)	GSP	GSP + AGV
SiO_2 (wt.%)	69.80	66.26	64.07	62.81	59.44
Al_2O_3 (wt.%)	11.83	12.93	14.33	14.05	15.01
Na_2O (wt.%)	2.31	2.46	2.67	2.62	3.29
K_2O (wt.%)	6.34	5.71	5.18	5.08	3.90
CaO (wt.%)	4.56	5.26	3.86	5.72	7.18
FeO (wt.%)	0.95	2.55	4.24	4.15	4.92
MgO (wt.%)	0.22	0.56	0.92	0.90	1.30
TiO_2 (wt.%)	3.91	4.06	4.42	4.36	4.54
MnO (wt.%)	0.06	0.06	0.04	0.04	0.06
P_2O_5 (wt.%)	0.02	0.15	0.27	0.27	0.36
Total	100.00	100.00	100.00	100.00	100.00
A/NK [a]	1.11	1.26	1.43	1.43	1.56
A/CNK [a]	0.62	0.65	0.84	0.70	0.66

[a] A/NK = $Al_2O_3/(Na_2O + K_2O)$, and A/CNK = $Al_2O_3/(Na_2O + K_2O + CaO)$, where oxides are molar.

Experimental Methods for Growth Experiments

- Starting material compositions were metaluminous and extend from trachydacite to rhyolite.
- Experiments run in Pt and $Ag_{60}Pd_{40}$ capsules in graphite wells in a piston-cylinder apparatus for 48-168 hours, 800-1000°C, H_2O 0-6 wt.%, and 0.5-1.0 GPa.
- fO2 close to CCO buffer, between IW and QFM.
- Experiments first heated to above the liquidus, then ramped down to the run temperature.
- Run products imaged and analyzed using a Tescan Vega 3 LM SEM with Oxford X-max EDS.
- Crystal-free areas of quenched glass analyzed with 10-15 µm diameter electron beam to minimize beam damage.

Growth Experiment Run Products

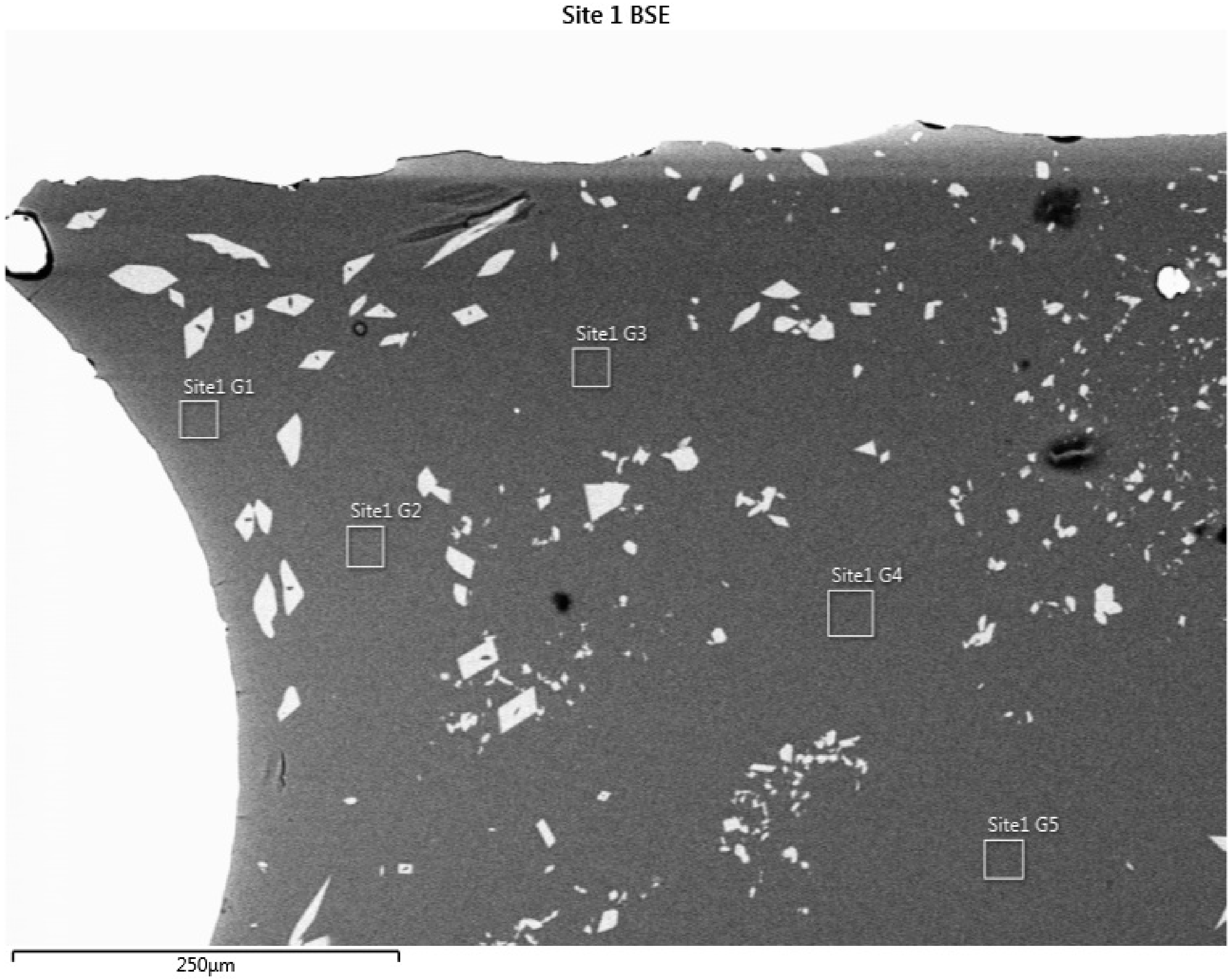

SpG.8, PST + GSP, T = 900°C, P = 0.5 GPa, H_2O = 3.8 wt.%

Growth Experiment Run Products

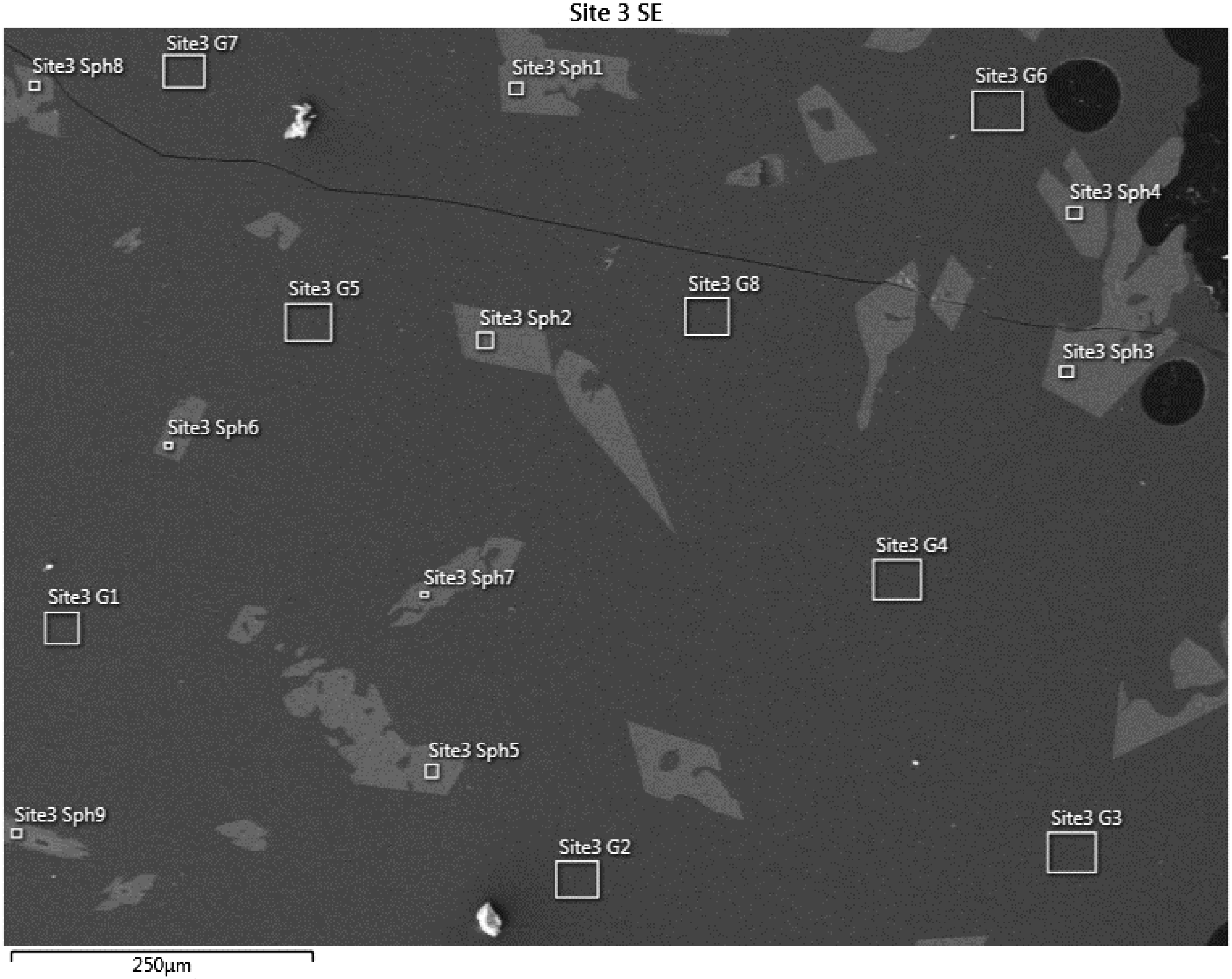

SpG.18, GSP + AGV, T = 900°C, P = 0.5 GPa, H_2O = 3.7 wt.%

SpG7: PST SM, 900°C, 4 wt. % H_2O, 168 h

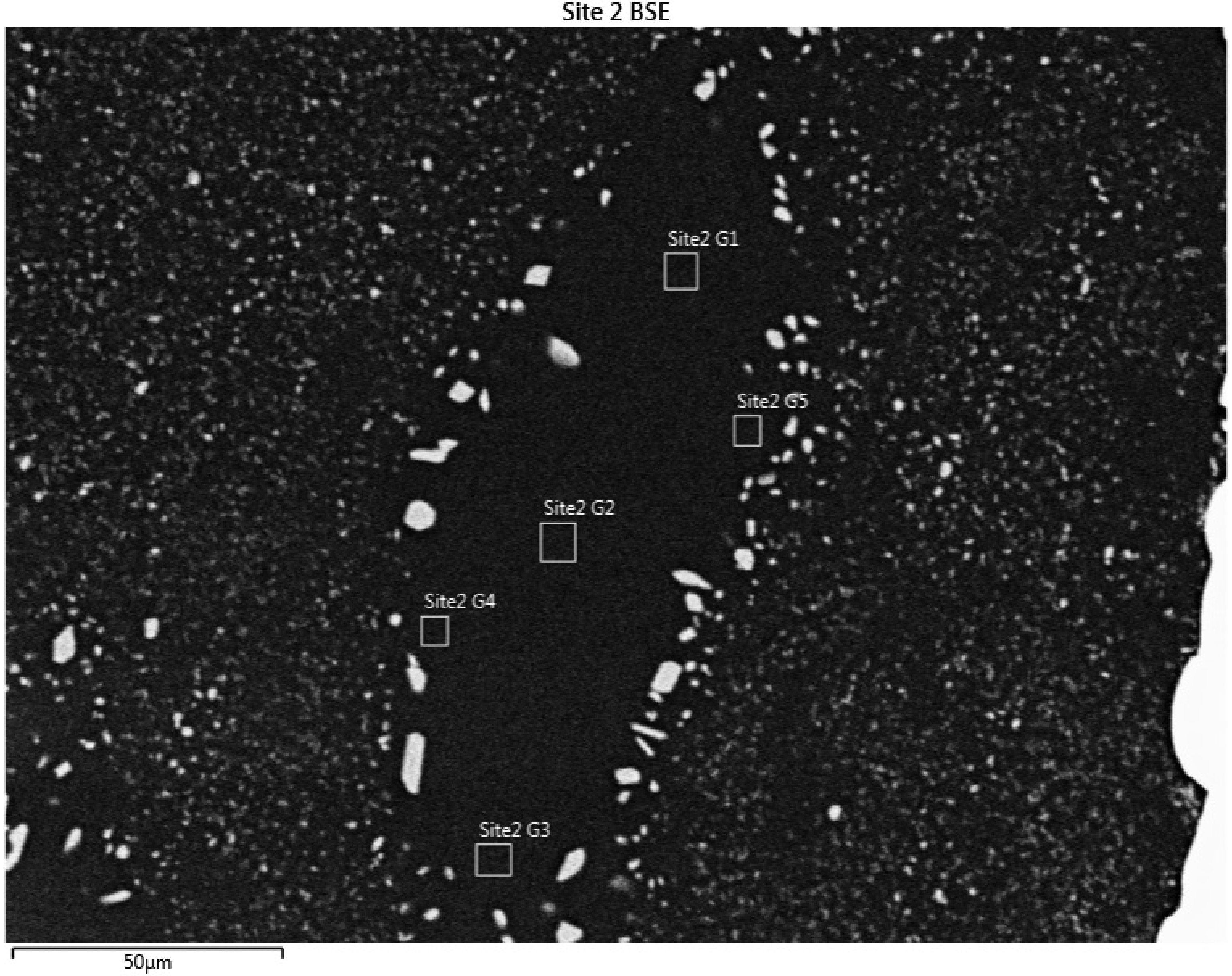

Assessment of EDS Accuracy

Oxide	GSP nom.	GSP meas.	% diff.	AGV-2 nom.	AGV-2 meas.	% diff.
n		13			13	
SiO_2	66.6	66.99	0.6%	59.3	59.66	0.6%
Al_2O_3	14.9	14.98	0.6%	16.91	17.08	1.0%
Na_2O	2.78	2.74	-1.4%	4.19	4.26	1.7%
K_2O	5.38	5.46	1.5%	2.88	2.94	2.1%
CaO	2.10	2.10	0.2%	5.20	5.12	-1.5%
Fe_2O_3	4.90	4.81	-1.8%	6.69	6.67	-0.3%
MgO	0.96	0.97	0.8%	1.79	1.80	0.6%
TiO_2	0.66	0.71	8.0%	1.05	1.06	1.4%
P_2O_5	0.29	0.26	-10.8%	0.48	0.46	-4.5%
Sum	98.57	99.02		98.49	99.06	

Glass Compositions, GSP SM, 1000°C

	GSP SM	DF–SpG.29		DF–SpG.33	
Capsule		AgPd		Pt	
Oxide	Conc. (wt.%)	Conc. (wt.%)	1σ	Conc. (wt.%)	1σ
SiO_2	67.96	66.21	0.38	68.29	0.03
Al_2O_3	15.20	15.81	0.38	15.62	0.01
Na_2O	2.78	3.14	0.07	2.98	0.01
K_2O	5.54	5.29	0.14	5.53	0.01
CaO	2.13	3.61	0.21	4.06	0.01
FeO (t)	4.39	3.19	0.16	0.04	0.004
MgO	0.98	0.82	0.04	1.00	0.004
TiO_2	0.72	1.66	0.08	2.21	0.02
MnO	0.03	0.04	0.004	0.03	0.003
P_2O_5	0.26	0.23	0.01	0.24	0.01
Sum		**100.00**		**100.00**	

Dissolution Experiments: SpDis.3 Run Products

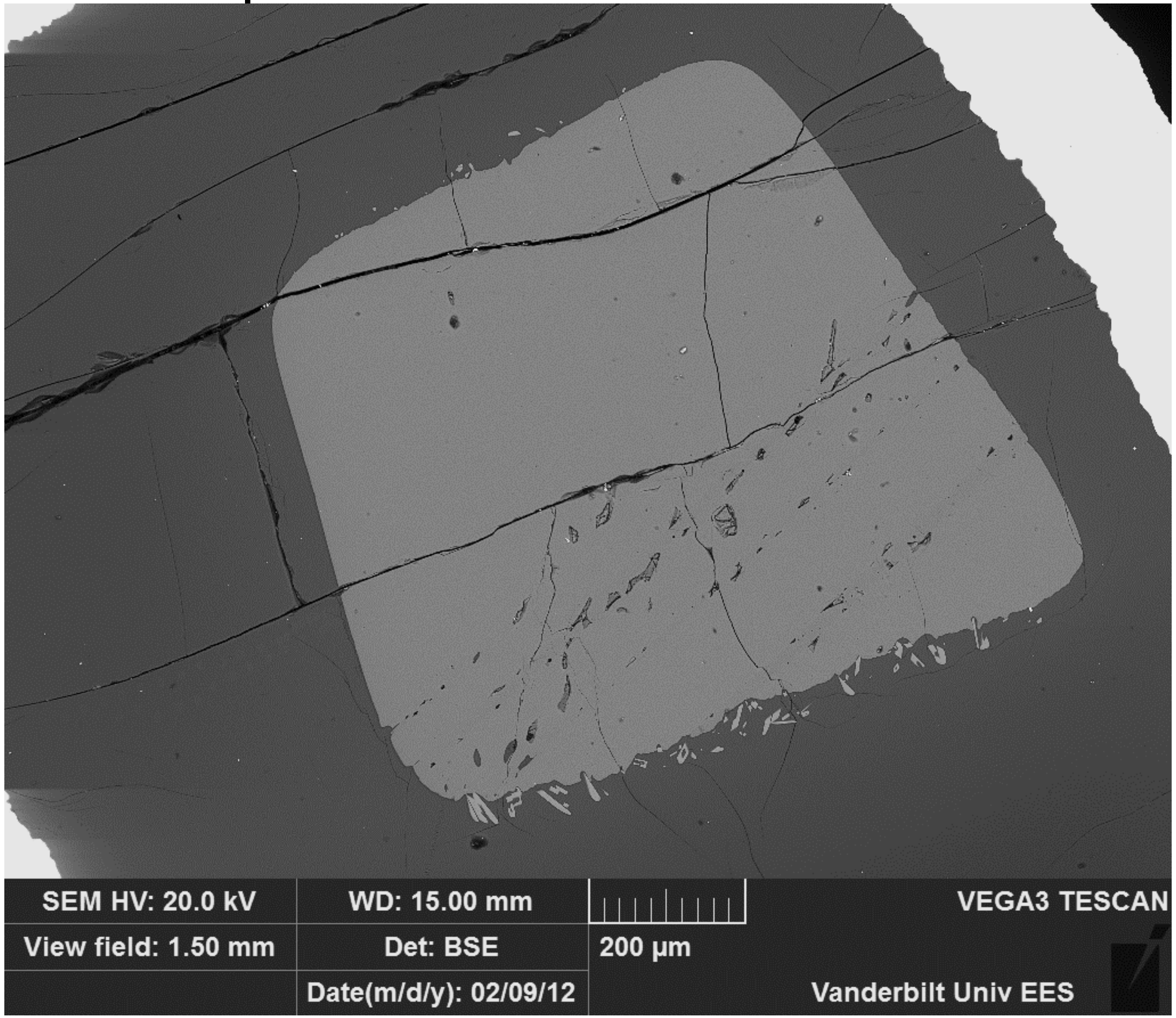

Evaluation of secondary fluorescence and precision

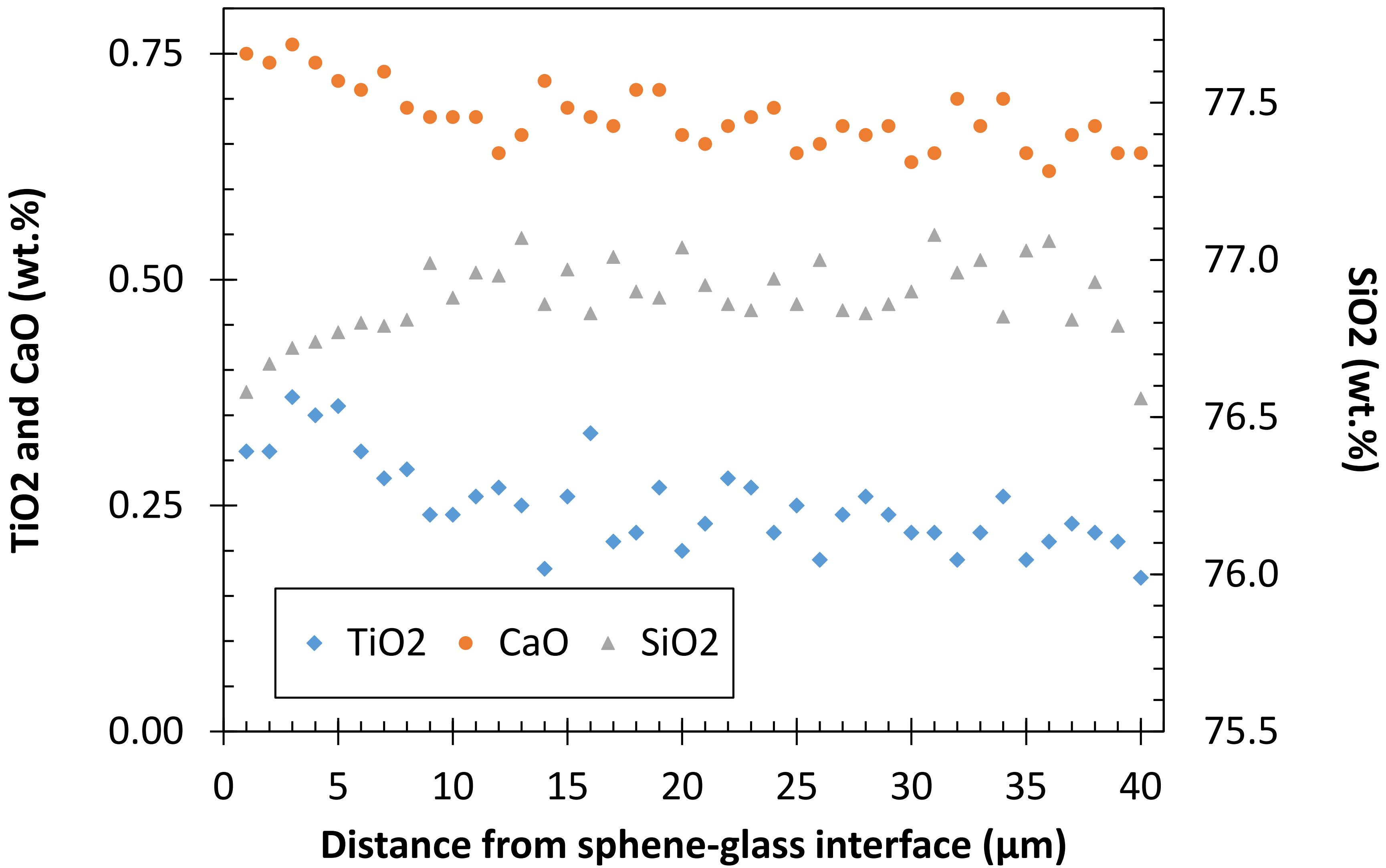

SpDis.2 Diffusion Profiles

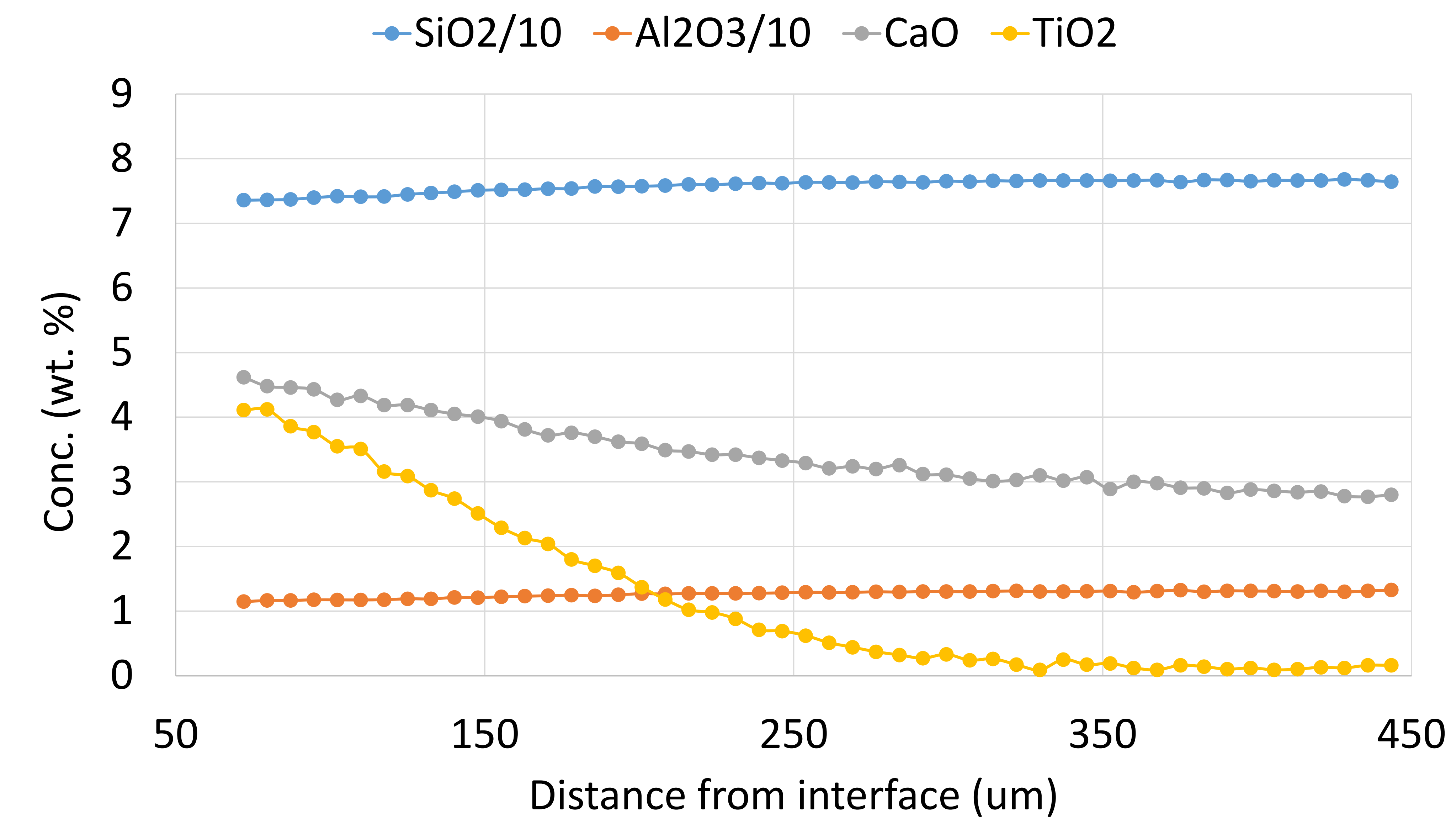

Diffusion profiles from dissolution experiments

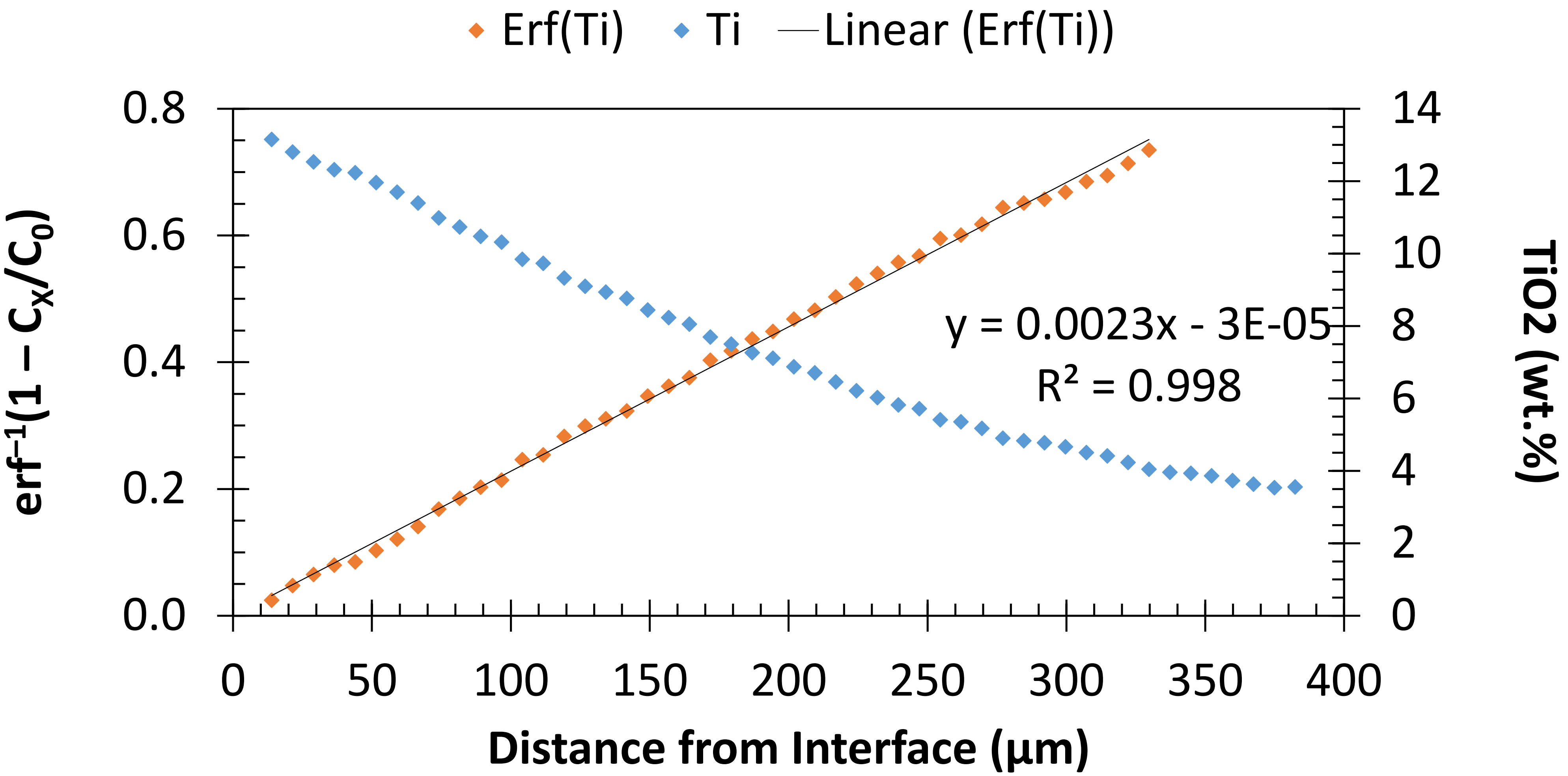

SphDis.3, T = 1300°C, P = 0.8 GPa, H_2O = 1.9 wt.%, duration = 18 h

Comparison of growth and dissolution experiment results

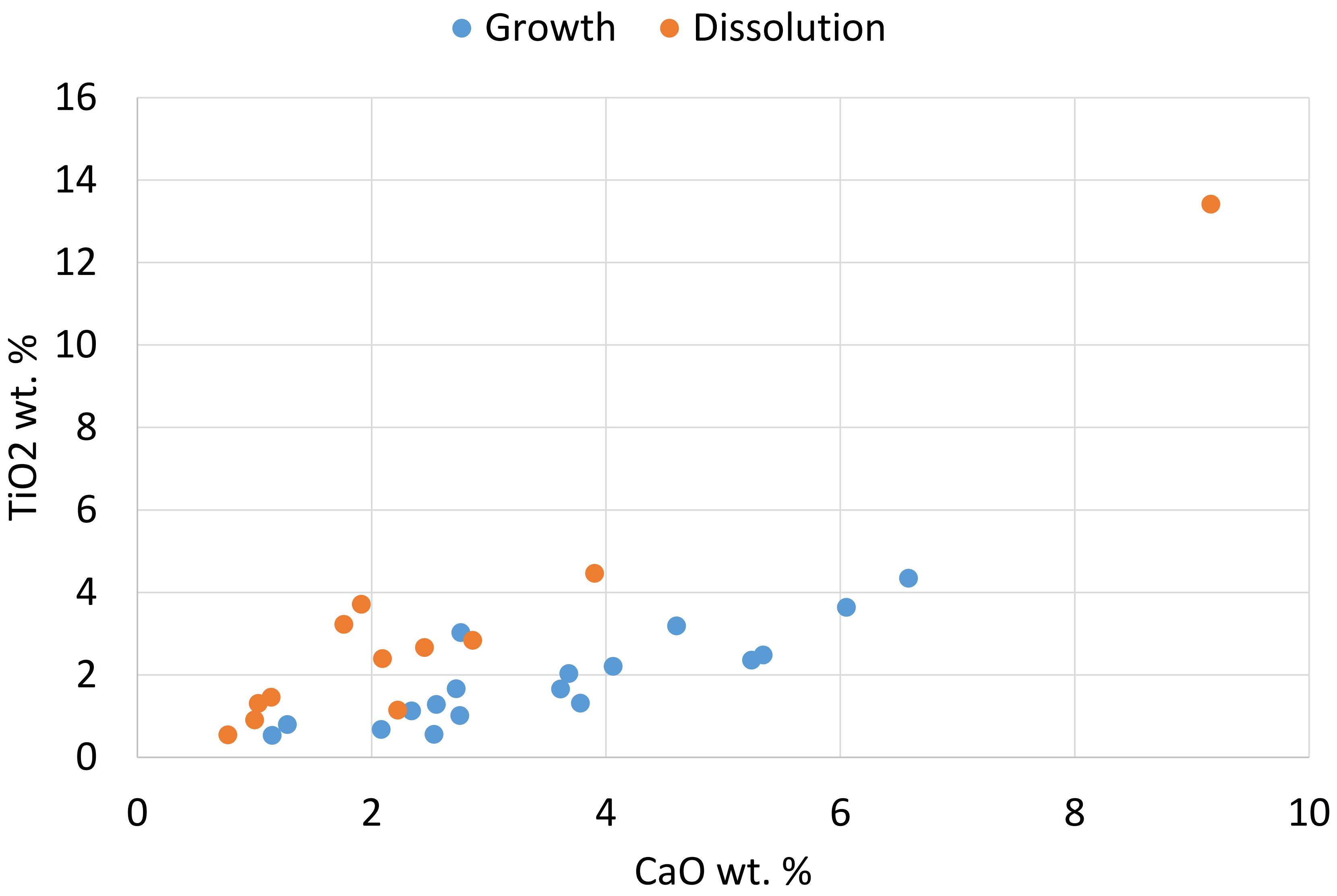

Solubility Equation

$$CaTiSiO_5^{sphene} = CaO^{melt} + TiO_2^{melt} + SiO_2^{melt}$$

- The activity of $CaTiSiO_5$ in sphene ~ 1. Thus,

$$\ln K = \ln [CaO]^{melt} + \ln [TiO_2]^{melt} + \ln [SiO_2]^{melt} = -\Delta G/RT$$

$$\ln C_{TiO2}^{melt} = -\Delta H/RT + \Delta S/R \; -\Delta V(P-1)/RT - \ln\gamma_{TiO2}^{melt} - \ln[CaO] - \ln[SiO_2]$$

- The last three terms are replaced by a single melt composition parameter C = (10* eCa)/(Al*Si), symbols are cation fractions, and excess calcium eCa = CaO - Al_2O_3 + Na_2O + K_2O with concentrations in moles
- Multiple linear regression of glass composition data from 23 growth and dissolution experiments yielded the sphene solubility equation (adj. r = 0.97):

TiO_2 (wt.%) = 0.79*C - 7993/T(K) + 7.88

Temperature dependence of sphene solubility

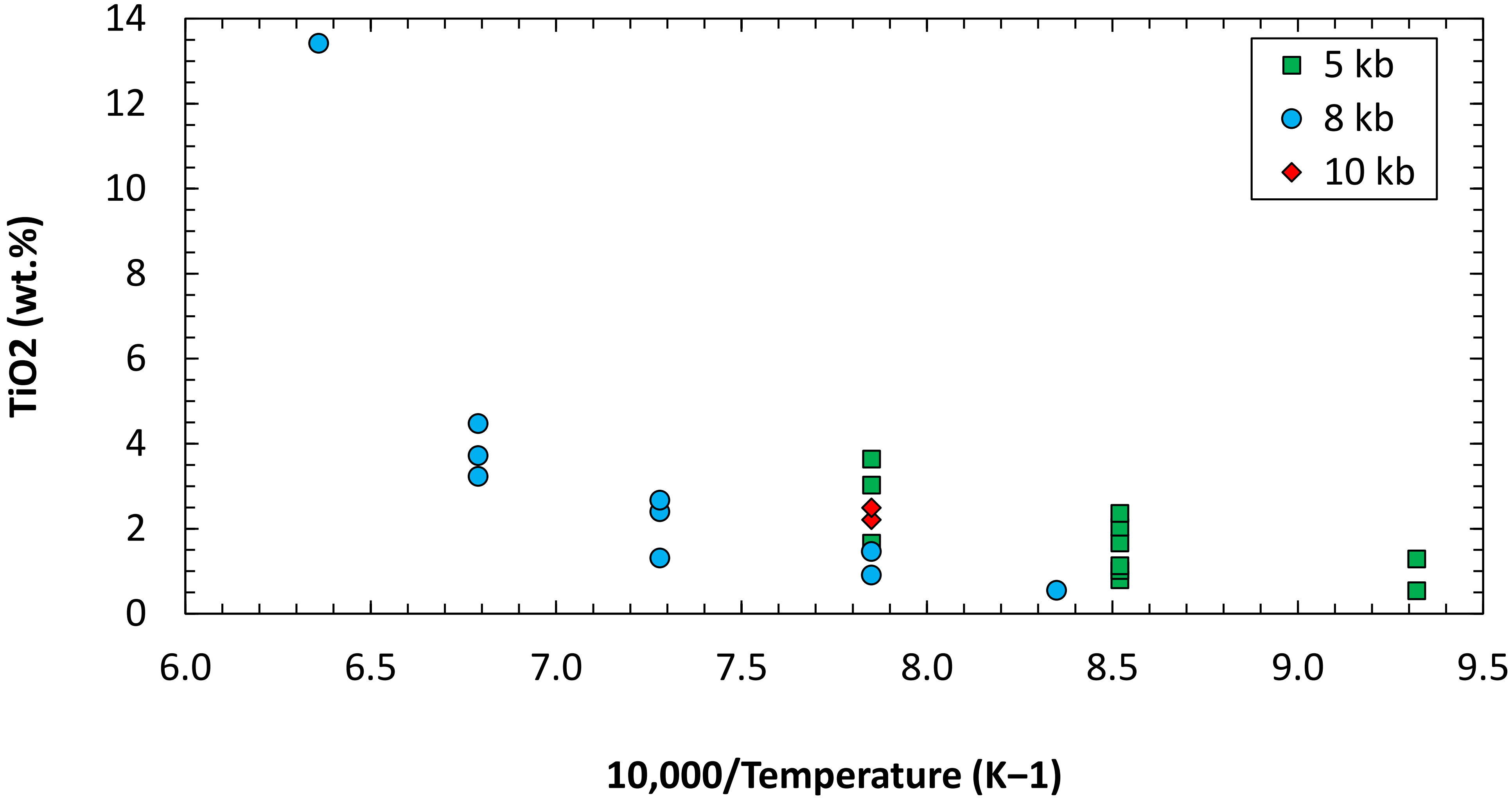

Dependence of sphene solubility on melt composition parameter C and T

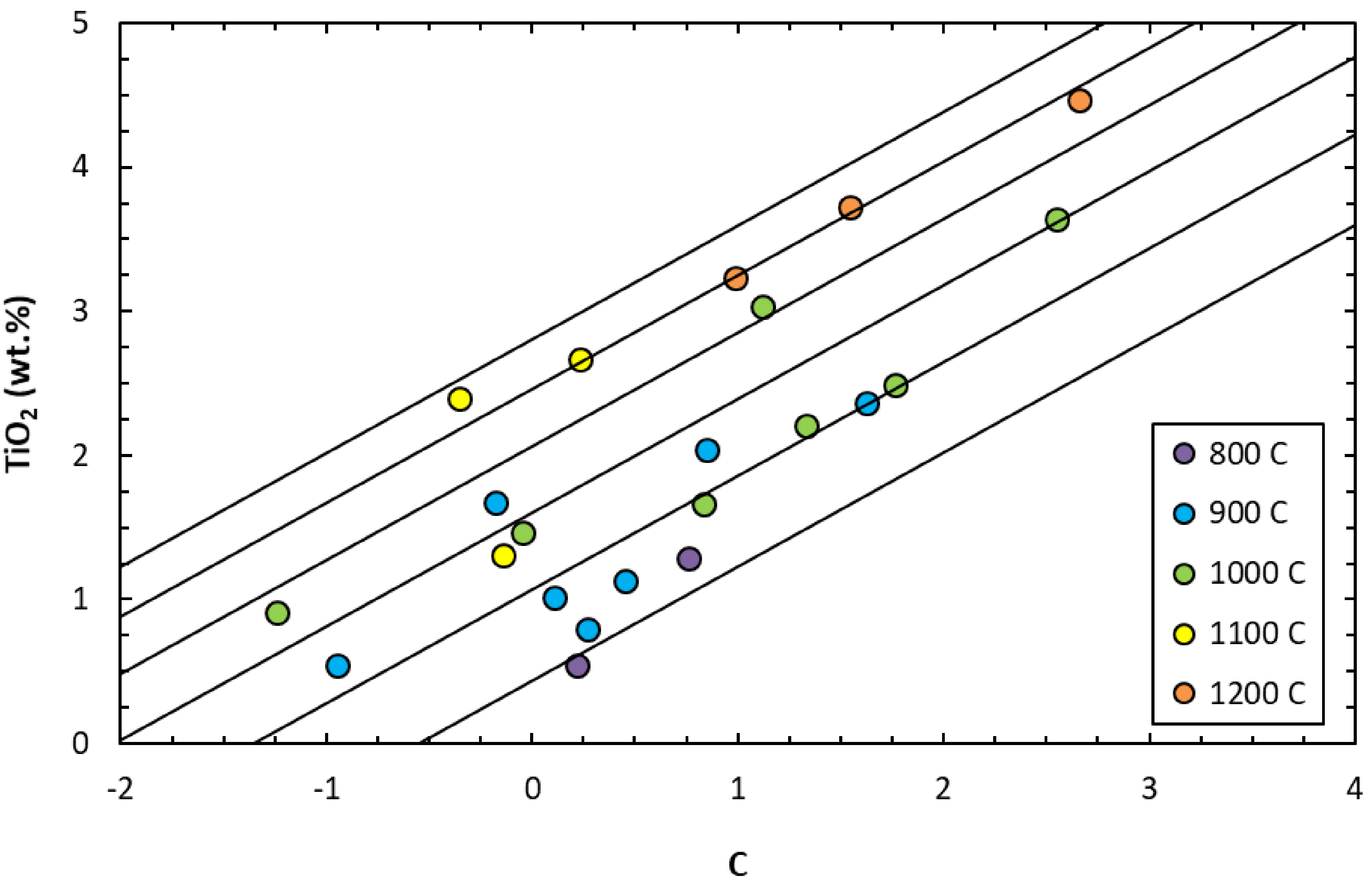

C = (10* eCa)/(Al*Si) and excess Ca eCa = CaO - Al_2O_3 + Na_2O + K_2O with concentrations in moles

Comparison to Sphene-bearing Natural Samples

Sample Name	Location[f]	Sample Type [a]	Zir. Sat. T (°C) W + H [b]	Sphene Sat. Temp. (°C) [c]	Remarks[e]
FCT intracaldera	Fish Canyon Tuff	glass	—	775	Fe-Ti oxide temp = 760 ± 30 °C
FCT outflow	Fish Canyon Tuff	glass	—	805	Fe-Ti oxide temp = 760 ± 30 °C
HRL16	Highland Range	glass	712	783	Zr-in-sphene T mostly 710-740 °C
HRL21	Highland Range	glass	734	787	Zr-in-sphene T mostly 710-740 °C
KPST01 [d]	Peach Spring Tuff	WR	809	742	Avg Zr-in-sph temps 770 ± 20 °C
PSTG [d]	Peach Spring Tuff	WR	901	819	Avg Zr-in-sph temps 770 ± 20 °C
WSW2 [d]	Peach Spring Tuff	WR	833	753	Avg Zr-in-sph temps 770 ± 20 °C

[a] glass = matrix glass, WR = whole-rock.

[b] Zircon solubility models: W + H—Watson and Harrison (1983), B et. al.—Boehnke et al. (2013). The Watson and Harrison temperatures are preferred due to the low resolution of the Boehnke et al. model at low temperatures.

[c] Solubility model of this study.

[d] The saturation temperature is an average of those calculated for each individual analysis and is not calculated from the average composition.

e Zr-in-sphene thermometer of Hayden et al. (2008).

f Bachmann et al (2002) for Fish Canyon Tuff, Colombini et al (2011) for Highland Range, Pamukcu et al (2013) for Peach Springs Tuff

Conclusions

- Sphene solubility in siliceous melts increases with increasing CaO/metaluminosity and increasing temperature.
- For the compositions and conditions studied, sphene solubility does not depend significantly on melt H_2O concentration or pressure.
- Results will be verified through reanalysis using an electron microprobe.
- We plan to compare sphene saturation temperatures calculated for natural samples to temperatures calculated using other thermometers.